Dynamic Structural Features of Macrocyclic Cytochalasin Analogues Responsible for Their Hexose Transport Inhibition

Satoru Goto,*,† Kai-Xian Chen,†,‡ Sanae Oda,† Hitoshi Hori,§ and Hiroshi Terada†

Contribution from the Faculty of Pharmaceutical Sciences, University of Tokushima, Shomachi 1-78, Tokushima 770, Japan, Institute of Materia Medica, Academia Sinica, Yue-yang Road 319, Shanghai 200031, China, and Biological Science and Technology, Faculty of Engineering, University of Tokushima, Minami-josanjima-cho 2-1, Tokushima 770, Japan

Received September 18, 1996. Revised Manuscript Received October 20, 1997

Abstract: For understanding the structural features of cytochalasin analogues necessary for hexose transport inhibition, we analyzed the conformations of the inhibitory cytochalasin B (CCB) and cytochalasin A (CCA) and the noninhibitory cytochalasin analogue 21,22-dihydrocytochalasin B ($CCBH_2$) by molecular mechanics computation. Results showed that the 3D-structures of these cytochalasin analogues are regulated by the α,β-unsaturated lactone moiety. Their global minimal conformers differed in the conformation of the lactone moiety. The populations of conformers having the same lactone moiety conformation as that of the global minimal conformer of CCB among the total possible conformers were 93% in CCB, 35% in CCA, and 0% in $CCBH_2$. As these populations were proportional to the magnitudes of the inhibitory effects of these analogues, we conclude that the most stable conformation of CCB with regard to the lactone moiety is the active conformation of cytochalasin analogues for hexose transport inhibition. Thus the conformation of cytochalasin analogues necessary for hexose transport inhibition could be deduced by this novel approach.

Introduction

Cytochalasin analogues, which are alkaloid fungal products, are well-known to inhibit hexose transport across various cell membranes.[1−6] Of these analogues, cytochalasin B (CCB) is the most potent, while cytochalasin A (CCA), in which the C(20)−OH moiety of CCB is replaced by C(20)═O, is about one-third as potent as CCB. However, 21,22-dihydrocytochalasin B ($CCBH_2$), in which the C(21), C(22) double bond of CCB is saturated, causes scarcely any inhibition (for chemical structures, see Chart 1). It is interesting that slight differences in the chemical structures of these analogues affect their inhibitory activities. As the effects of CCB and CCA are competitive with that of the transport substrate glucose, the structural requirements for hexose transport inhibition have previously been studied mainly with regard to common structural features of CCB, CCA, and D-glucose.[7−9]

Chart 1. Chemical Structures of Cytochalasin A (CCA), Cytochalasin B (CCB) and 21,22-Dihydrocytochalasin B ($CCBH_2$)

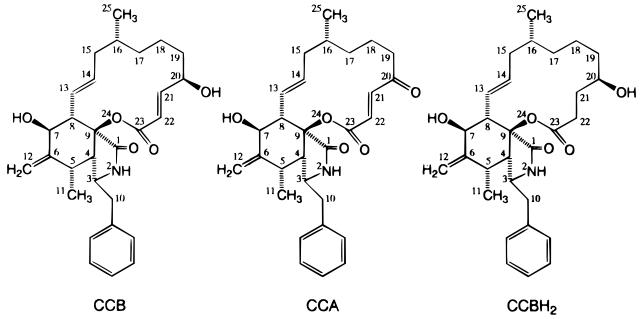

Taylor and Gagneja[7] proposed that the O(24) and the oxygen atoms attached to C(1), C(20), and C(23) are responsible for the stereospecific binding of CCB with the glucose transporter, based on the structures common to those of the transport substrate D-glucose, and the transport inhibitors phenolphthalein, hydrocortisone, corticosterone, predonisolone, and 11β-hydroprogesterone. From the 3-D structures based on X-ray crystallographic studies of cytochalasins and chaetoglobosin analogues, in which the benzyl ring of cytochalasins is replaced by an

* Corresponding author. Fax: +81-886-33-5192. E-mail: sgoto@ph.tokushima-u.ac.jp.

† Faculty of Pharmaceutical Sciences, University of Tokushima.

‡ Institute of Materia Medica, Academia Sinica.

§ Biological Science and Technology, Faculty of Engineering, University of Tokushima.

(1) Lin, S.; Santi, D. V.; Spudich, J. A. Biochemical studies on the mode of action of cytochalasin B. Preparation of tritiated cytochalasin B and studies on its binding of cells. In *J. Biol. Chem.* **1974**, *249*, 2268−2274.

(2) Lin, S.; Spudich, J. A. Biochemical studies on the mode of action of cytochalasin B. Cytochalasin B binding to red cell membrane are in relation to glucose transport. In *J. Biol. Chem.* **1974**, *249*, 5778−5783.

(3) Lin, S.; Spudich, J. A.; Binding of cytochalasin B to a red cell membrane protein. In *Biochem. Biophys. Res. Commun.* **1974**, *61*, 1471−1476.

(4) Jung, C. Y.; Rampal, A. L. Cytochalasin B binding sites and glucose transport carrier in human erythrocyte ghosts. In *J. Biol. Chem.* **1977**, *252*, 5456−5463.

(5) Horne, M. K.; Hart, J. S. Cytochalasin inhibition of hexose transport by platelets. In *Biochim. Biophys. Acta* **1987**, *903*, 349−357.

(6) Pessin, J. E.; Tillotson, L. G.; Yamada, K.; Gitomer, W.; Carter, Su. C.; Mora, R.; Isselbacher, K. J.; Czech, M. P. Identification of the stereospecific hexose transporter from starved and fed chicken embryo fibroblasts. In *Proc. Natl. Acad. Sci. U.S.A.* **1982**, *79*, 2286.

(7) Taylor, N. F.; Gagneja, G. L. A model for the mode of action of cytochalasin B inhibition of D-glucose transport in the human erythrocyte. In *Can. J. Biochem.* **1975**, *53*, 1078−1084.

(8) Rampal, A. L.; Pinkofsky, H. B.; Jung, C. Y. Structure of cytochalasins and cytochalasin B binding sites in human erythrocyte membranes. In *Biochemistry* **1980**, *19*, 679−683.

(9) Griffin, J. F.; Rampal, A. L.; Jung, C. Y. Inhibition of glucose transport in human erythrocytes by cytochalasins: A model based on diffraction studies. In *Proc. Natl. Acad. Sci. U.S.A.* **1982**, *79*, 3759−3763.

S0002-7863(96)03287-8 CCC: $15.00
Published on Web 02/25/1998

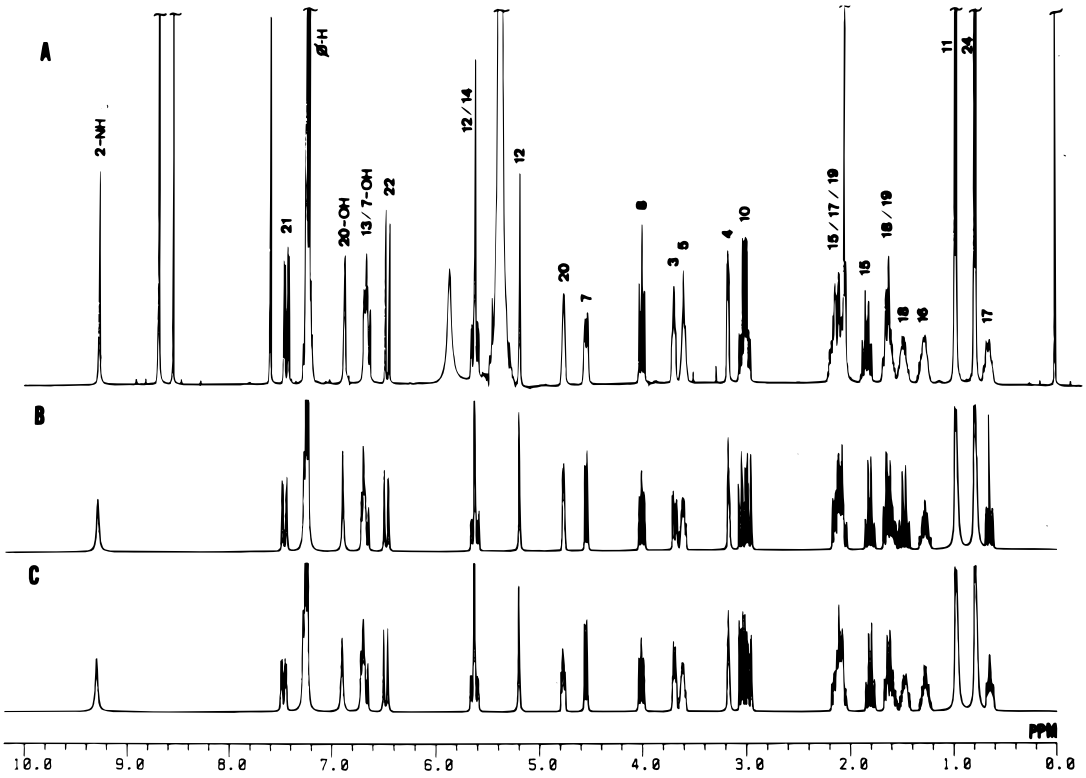

Figure 1. ^{1}H NMR spectrum of cytochalasin A and its simulated spectra. (A) 400 MHz ^{1}H NMR spectrum of CCB (20 mg/mL) recorded in pyridine-d_5 at room temperature. Assigned signals are shown as position numbers beside signals according to the COSY spectrum. (B) Simulation spectrum according to the optimized structure of CCB. Simulation was performed with the parameters chemical shift (δ) and the geminal coupling constant ($^2J_{HH}$) from the experimental spectrum, and vicinal ($^3J_{HH}$) and long range ($^4J_{HH}$) coupling constants were calculated according to Karplus-type equations (J_{calc})[14,15] from the optimized structure of CCB. C: Simulated spectrum according to parameters based on the results of dynamic conformational analysis. Simulation was performed from the values for experimental δ and computed J_{ave}.

indole ring, Jung's group[8,9] found that the α,β-unsaturated lactone moiety and hydrogenated isoindole ring are superimposable on D-glucose, and hence concluded that these regions are important for binding to the glucose transporter and inhibition of glucose transport. These similarities appear to explain the inhibitory activities of CCB and CCA. However, they do not explain why $CCBH_2$ is not inhibitory. Since the reports by Jung's group, there seem to have been no studies on the structure−bioactivity relationships of cytochalasin analogues for more than a decade, although CCB and CCA have been commonly used as hexose transport inhibitors in biochemical studies. Therefore, it is necessary to determine the structural features necessary for hexose transport inhibition.

In the present study, we determined the dynamic structures of CCB, CCA, and $CCBH_2$. We performed molecular mechanics (MM) computation of these analogues for determination of the populations of the conformation that was effective for hexose transport inhibition by conformational population analysis developed by us[10,11] using the MM calculation program CONFLEX3.[12] In this way we determined the structure of CCB and CCA necessary for their inhibitory action. The results showed why CCB is more potent than CCA, and why $CCBH_2$ is ineffective.

(10) Goto, S.; Guo, Z. R.; Futatsuishi, Y.; Hori, H.; Taira, Z.; Terada, H. Quantitative structure−activity relationships of benzamide derivatives for anti-leukotriene activities. In *J. Med. Chem.* **1992**, *35*, 2440−2445.

(11) Terada, H.; Goto, S.; Hori, H.; Taira, Z. *Structure requirements of leukotriene antagonists, QSAR and Drug Design−New Developments and Applications*; Fujita, T., Ed.; Elsevier: Amsterdam, 1995; pp 341−367.

(12) Goto, H.; Osawa, E. An efficient algorithm for searching low-energy conformers of cyclic and acyclic molecules. In *J. Chem. Soc., Perkin Trans. 2* **1993**, 187−198.

Results

1. ^{1}H NMR Spectra of Cytochalasins B and A and Their Simulations. First, we tried to determine the 3-D structures of cytochalasin analogues in aqueous solution by NMR spectroscopy. As cytochalasin analogues were hardly soluble in water, we recorded their ^{1}H NMR spectra in pyridine solution. This might make direct analysis of the dynamic structures of cytochalasin analogues in aqueous solution difficult. As described below, however, we simulated the NMR spectra well by a computational approach. Therefore, the structures of the cytochalasin analogues we determined were probably not far from those in aqueous solution.

Figure 1A shows the NMR spectrum of the potent hexose transport inhibitor CCB in pyridine-d_5 at room temperature. Assignment of NMR signals was carried out from the ^{1}H,^{1}H-COSY spectrum, and the values of the coupling constant J, referred to as J_{obs}, are summarized in Table 1. The apparent singlet signal of C(20) methine at 4.77 ppm should consist of multiple peaks due to its coupling with the protons of C(19), C(20)−OH, C(21), and C(22). For analysis of the overlapping signals due to the hydrocarbon chain C(19)−C(18)-C(17)−C(16)−C(15)−C(14)═C(13)−C(8)−C(7), we measured the NMR spectrum at the higher temperature of 50 °C (data not shown), and determined the J_{obs} values. These values were confirmed by signal decoupling by pulse irradiation at room temperature.

The complete data set of geometrical coordinates for CCB has not been reported, and its reported crystal structure has either been incomplete[13] or that of a complex with $AgBF_4$.[14] Therefore, we constructed the optimized structure of CCB shown in Figure 2 by MM calculation according to the reported proce-

Table 1. ^{1}H,^{1}H Coupling Constants of CCB and CCA[a]

^{1}H−^{1}H pairs	CCB			CCA		
	J_{obs}	J_{calc}	J_{ave}	J_{obs}	J_{calc}	J_{ave}
H−C(3)−C(4)−H	4.9	4.3	3.2	4.3	4.8	5.6
H−C(4)−C(5)−H	2.9	3.2	3.6	7.9	2.9	2.8
H−C(7)−C(8)−H	10.2	9.3	9.1	9.8	9.5	10.6
H−C(8)−C(13)−H	10.2	11.6	11.2	11.6	10.7	10.5
H−C(13)═C(14)−H	15.5	16.0	16.1	14.7	16.0	16.0
H−C(13)═C(14)−C(15)−H	n.d.	2.2	1.2	1.8	1.3	0.9
H−C(8)−C(13)═C(14)−H	n.d.	1.3	1.1	1.8	0.9	0.9
H−C(14)−C(15)−H(a)[b]	3.4	3.2	3.7	3.1	3.1	3.5
H−C(14)−C(15)−H(b)[b]	11.2	11.6	11.3	11.0	11.5	10.7
H(a)−C(15)−H(b)[b]	13.2	13.2[c]	13.2[c]	14.0	14.0[d]	14.0[d]
H(b)−C(15)−C(16)−H[b]	13.2	12.4	11.1	11.0	12.1	11.2
H(a)−C(17)−H(b)[b]	n.d.	14.0[d]	14.0[d]	13.4	14.0[d]	14.0[d]
H(a)−C(17)−C(18)−H(a)[b]	n.d.	12.9	9.8	8.6	5.5	6.0
H(a)−C(17)−C(18)−H(b)[b]	n.d.	3.4	5.2	8.6	1.9	6.0
H(b)−C(17)−C(18)−H(b)[b]	n.d.	12.9	11.6	13.4	13.0	9.3
H(b)−C(17)−C(18)−H(a)[b]	n.d.	1.8	3.7	8.5	2.0	4.9
H(a)−C(19)−H(b)[b]	n.d.	14.0[d]	14.0[d]	14.0	14.0[d]	14.0[d]
H(a)−C(18)−C(19)−H(a)[b]	n.d.	12.2	9.0	11.0	13.0	10.8
H(a)−C(18)−C(19)−H(b)[b]	n.d.	7.4	10.0	7.3	5.4	7.5
H(b)−C(18)−C(19)−H(a)[b]	n.d.	0.9	1.6	3.1	1.8	2.7
H(b)−C(18)−C(19)−H(b)[b]	n.d.	1.0	1.6	2.4	2.0	2.8
H−C(21)═C(22)−H	15.6	16.1	16.1	15.9	16.1	16.0
H−C(20)−C(21)−H	4.4	3.3	5.0			
H−C(20)−C(21)═C(22)−H	1.5	2.1	1.2			
H−C(20)−O−H	3.4	0.5	0.5			
H(a)−C(10)−H(b)[b]	13.8	13.8[c]	13.8[c]	13.4	13.4[c]	13.4[c]
H−C(3)−C(10)−H(a)[b]	7.3	11.8	8.0	8.6	11.9	11.5
H−C(3)−C(10)−H(b)[b]	6.2	2.2	3.4	2.2	2.4	2.5
H−C(5)−C(11)−H	6.8	6.8[c]	6.8[c]	6.7	6.7[c]	6.7[c]
H−C(16)−C(25)−H	6.3	6.3[c]	6.3[c]	6.7	6.7[c]	6.7[c]

[a] J_{obs} was determined from the recorded NMR spectrum. J_{calc} was determined from the crystal structure of CCA and optimized structure of CCB. n.d. = not determined. [b] H(a) and H(b) of CCB represent the proton signals at δ of 3.0 (3.04) and 3.0 (2.99) ppm for C(10), at δ of 2.1 and 1.8 ppm for C(15), at δ of 1.5 and 1.6 ppm for C(18), and at δ of 1.6 and 2.1 ppm for C(19), respectively. H(a) and H(b) of CCA represent protons of the signals at δ 3.3 and 3.1 ppm for C(10), 2.2 and 2.0 ppm for C(15), 1.8 and 1.0 ppm for C(17), 1.6 and 1.5 ppm for C(18), and 2.6 and 2.4 ppm for C(19), respectively. [c] J values of geminal and vicinal coupling constants determined experimentally. [d] Optimized J value of geminal protons based on reported values.[17]

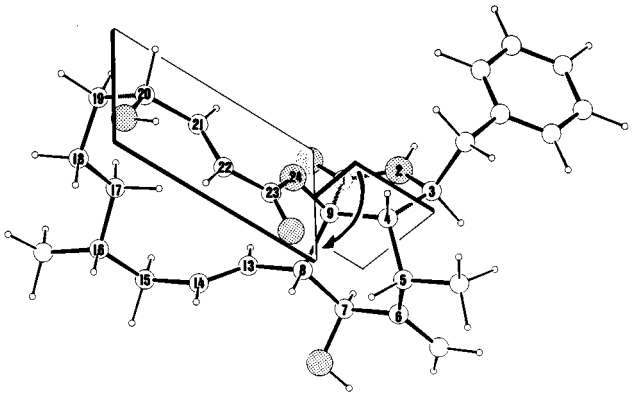

Figure 2. Most stable conformation of CCB. Carbon atoms and hydrogen atoms are shown by open circles and the heteroatoms nitrogen and oxygen by shadowed circles. The conformational search was performed with a CONFLEX3 program. The conjugated plane of the lactone moiety and the reference plane O(24)−C(9)−C(4) are shown by rectangles. Anticlockwise orientation of these planes is shown by an arrow.

dure.[12] The positional parameters of this conformer shown by dihedral angles are summarized in Table 2 and agree well with those obtained from the published crystal structure.[13] The structure is very similar to that of the CCB−$AgBF_4$ complex.[14]

Table 2. Dihedral Angles in the Structures of CCA, CCB, and $CCBH_2$

defining atoms	dihedral angle				
	crystal		calculated		
	CCB	CCA	CCB	CCA	$CCBH_2$
C(9)−C(1)-N(2)−C(3)	3.4	−11.4	−2.3	−2.1	−6.0
C(1)−N(2)−C(3)−C(4)	−2.5	8.7	0.3	−2.7	−1.6
N(2)−C(3)−C(4)−C(5)	115.0	120.4	125.8	130.5	133.1
C(3)−C(4)−C(9)−C(8)	125.1	119.1	117.6	113.0	107.9
C(3)−C(4)−C(5)−C(6)	−68.7	−64.3	−66.5	−63.8	−63.2
C(4)−C(5)−C(6)−C(7)	−58.8	−49.1	−51.4	−48.5	−42.5
C(5)−C(6)−C(7)−C(8)	11.7	−7.5	−1.7	−5.2	−12.9
C(6)−C(7)−C(8)−C(9)	44.1	57.8	52.5	53.0	55.7
C(7)−C(8)−C(9)−C(1)	65.2	67.3	67.2	72.4	75.6
N(2)−C(1)−C(9)−C(4)	−2.8	8.9	3.2	5.9	10.7
C(7)−C(8)−C(13)−C(14)	136.2	124.7	116.4	132.7	142.4
C(8)−C(13)−C(14)−C(15)	171.1	−178.0	−179.9	−174.7	−176.1
C(13)−C(14)−C(15)−C(16)	−129.1	−114.6	−125.9	−135.1	−135.2
C(14)−C(15)−C(16)−C(17)	76.6	70.9	62.0	77.1	103.9
C(15)−C(16)−C(17)−C(18)	−165.2	−172.6	−167.0	−163.7	−179.9
C(16)−C(17)−C(18)−C(19)	172.7	57.9	175.4	72.0	58.4
C(17)−C(18)−C(19)−C(20)	−101.4	78.4	−82.4	73.1	47.9
C(18)−C(19)−C(20)−C(21)		−58.1	61.2	−87.1	178.2
C(19)−C(20)−C(21)−C(22)		144.9	−122.3	175.9	150.9
C(20)−C(21)−C(22)−C(23)		−171.7	177.6	−175.7	40.2
C(21)−C(22)−C(23)−O(24)		−5.4	−2.5	0.6	−112.0
C(22)−C(23)−O(24)−C(9)		162.8	−159.7	−28.2	172.0
C(23)−O(24)−C(9)−C(8)		−165.3	57.8	−164.7	−163.2
C(4)−C(3)−C(10)−C(26)	51.4	62.5	−172.4	−171.3	−163.9
C(3)−C(10)−C(26)−C(27)	88.4	83.3	90.7	90.9	92.7

We calculated the J values (J_{calc}) according to Karplus-type equations,[15−17] as shown in Table 1, from the optimized structure of CCB (Figure 2). Then, we simulated the NMR spectrum of CCB based on the J_{calc} and chemical shift (δ) of the NMR spectrum, as shown in Figure 1B. In the simulated spectrum, the signal patterns due to the C(17) and C(18) methylenes at δ 0.65 and 1.47 ppm, respectively, were not the same as those of the observed spectrum shown in Figure 1A, indicating that the values of J_{calc} with regard to the global minimum structure of CCB were not sufficient to explain the experimental spectrum due to a difference in conformation between the crystalline and soluble states.

Figure 3A shows the ^{1}H NMR spectrum of CCA recorded under identical conditions as those employed for CCB. We assigned the NMR signals from the ^{1}H,^{1}H-COSY and NOESY spectra (data not shown), and the values of J_{obs} are summarized in Table 1. The correlation peaks of the NOESY spectrum are consistent with the crystal structure of CCA reported by Griffin et al.[9] The most stable structure of CCA optimized by MM calculation,[10−12] shown in Figure 4, agrees well with its crystal structure.[8,9] The dihedral angles of CCA in the crystal and its optimized structure are summarized in Table 2. We next determined the J_{calc} values using the same procedure as for determination of those of CCB. These values, shown in Table 1, are in general consistent with the corresponding J_{obs} values.

(13) Beno, M. A.; Cox, R. H.; Wells, J. M.; Cole, R. J.; Kirksey, J. W.; Christoph, G. G. Structure of a new [11]cytochalasin, cytochalasin H or Kodo-cytochalasin-1. In *J. Am. Chem. Soc.* **1977**, *99*, 4123−4130.

(14) McLaughlin, G. M.; Sim, G. A. The absolute stereochemistry of phomin: X-ray analysis of the phomin−silver fluoroborate complex. In *Chem. Commun. (J. Chem. Soc.)* **1970**, 1398−1399.

(15) Haasnoot, C. A. G.; de Leeuw, F. A. A. M.; Altona, C. The relationship between proton−proton NMR coupling constants and substituent electronegativities-I. In *Tetrahedron* **1980**, *36*, 2783−2792.

(16) Garbisch, E. W., Jr. Conformations. VI. Vinyl−allylic proton spin couplings. In *J. Am. Chem. Soc.* **1964**, *86*, 5561−5564.

(17) Jackman, L. M.; Sternhell, S. *Applications of Nuclear Magnetic Resonance Spectroscopy in Organic Chemistry*, 2nd ed.; Pergamon Press: London, 1969.

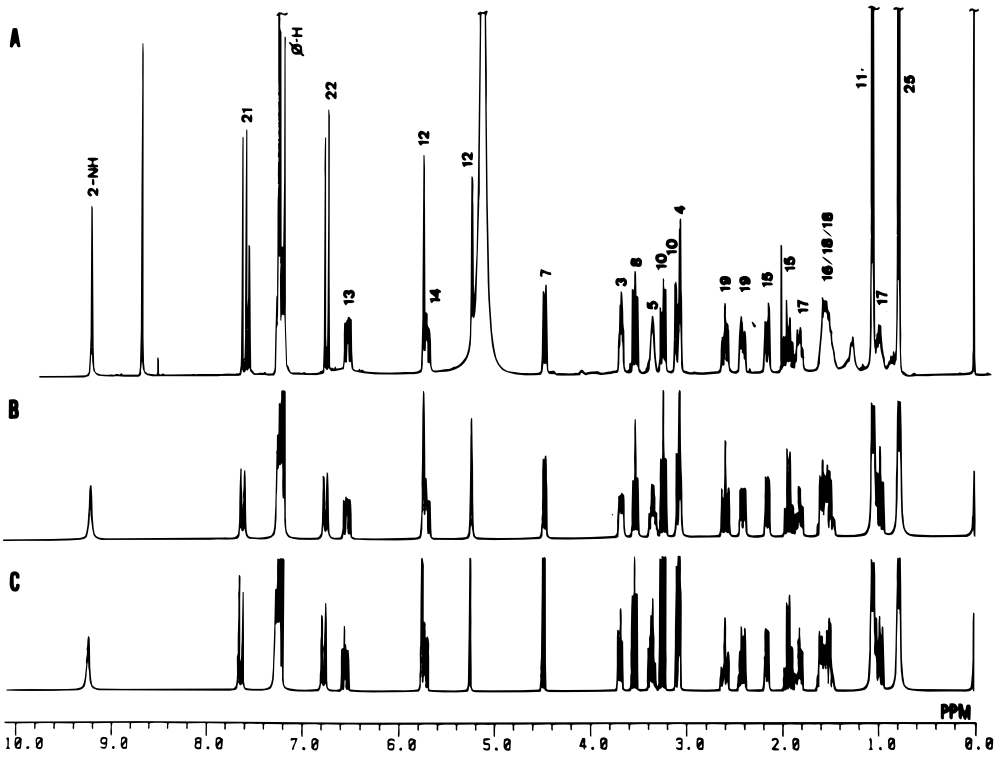

Figure 3. ^{1}H NMR spectrum of cytochalasin A and its simulated spectra. (A) Spectrum recorded under the same conditions as those described in Figure 1. (B) Simulation spectrum according to the crystal structure of CCA.[9] Simulation was performed with δ and $^2J_{HH}$ from the observed spectrum, and $^3J_{HH}$ and $^4J_{HH}$ were calculated according to Karplus-type equations (J_{calc})[14,15] from the crystal coordinates of CCA.[9] (C) Simulated spectrum according to parameters based on the results of dynamic conformational analysis. Simulation was performed as for Figure 1C.

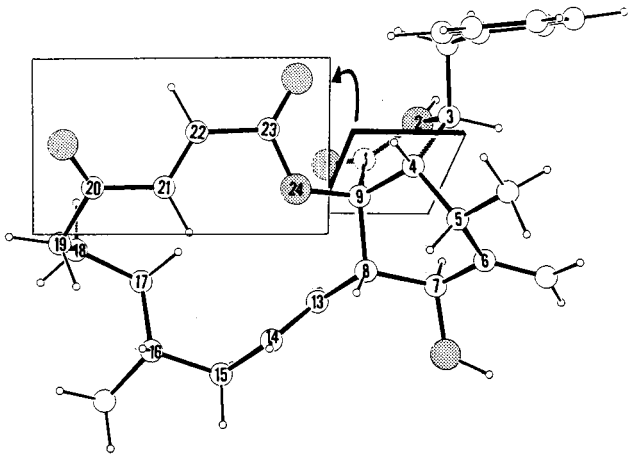

Figure 4. Most stable conformation of CCA. Clockwise orientation of α,β-unsaturated lactone moiety with respect to the O(24)−C(9)−C(4) plane is shown by an arrow. For details, see the legend of Figure 2.

The difference between the J_{calc} (2.9 Hz) and J_{obs} (7.9 Hz) of the C(4) and C(5) methine signals was due to overlapping with one of the C(10) methylene signals.

Figure 3B shows the simulated ^{1}H NMR spectrum of CCA determined on the basis of the J_{calc} values and the observed δ. The simulated spectrum as a whole appeared to fit the experimental spectrum well. However, besides the coupled C(4) and C(5) methine signals described above, the signal due to C(3) methine was different from that of the experimental spectrum shown in Figure 3A, because the apparent coupling constant of the C(3) methine signal was derived from the average free rotation of the C(3)−C(10) bond. In addition, as observed in the simulated spectrum of CCB, the multiplet signals due to C(16), C(17), C(18), and C(19) protons of the macrocyclic ring of CCA were not simulated well, possibly owing to their interaction with the α,β-unsaturated lactone moiety, as described later.

In the optimized structure of CCA (Figure 4), the α,β-unsaturated lactone moiety is located close to the benzyl group attached to the C(3) atom, restricting the free rotation of C(3)−C(10) in solution. This effect was determined by the difference between the δ values ($\Delta\delta(CH_2)$) of the C(10) methylene geminal protons. The $\Delta\delta(CH_2)$ value of the two signals due to C(10) methylene geminal protons was 0.15 ppm (64 Hz) for CCA and 0.06 ppm (24 Hz) for CCB. The higher $\Delta\delta(CH_2)$ value for CCA indicates that the rotation of its C(3)−C(10) bond was more restricted than that in CCB due to steric hindrance by the α,β-unsaturated lactone moiety.

In the optimized structure of CCB (Figure 2), the α,β-unsaturated lactone moiety is located closer to the hydrocarbon chain of the 14-membered macrocyclic ring than the C(3)-benzyl group. This geometry should be observed as an anisotropic field effect of the circular current of π-electrons around the α,β-unsaturated lactone moiety on one of the methylene protons of the macrocyclic ring. In fact, the $\Delta\delta(CH_2)$ value of 1.44 ppm (574 Hz) of the geminal protons due to the C(17) methylene of CCB was greater than that of 0.85 ppm (339 Hz) of CCA. Therefore, the α,β-unsaturated lactone moiety was closer to the C(17) methylene of CCB than of CCA. In addition, the difference in the multiplet signals of C(17) methylene and C(18) methylene at high magnetic field (δ 0.65 and 1.47 ppm, respectively) in the observed NMR spectrum of CCB (Figure 1A), from the triplet and quartet signals in the simulated spectrum (Figure 1B), indicates that the methylene groups of the macrocyclic ring of CCB fluctuate in solution. Therefore, conformational change should be taken into account for more complete simulations of the NMR spectra of CCB and CCA.

2. 3-D Structures of Cytochalasins B and A. As the proton

Table 3. Populations of Possible Conformers of CCB, CCA, and $CCBH_2$ Determined by Conformational Population Analysis

		CCB 3,072[a]	CCA 6,578[a]	$CCBH_2$ 3,195[a]
n ($\Delta E_i \leq 3$ kcal/mol)[b]		82	61	33
P_{total} ($\Delta E_i \leq 3$ kcal/mol)[c]		98.8%	96.3%	97.9%
n ($\Delta E_i \leq 50$ kcal/mol)[d]		496	494	495
P_{total} ($\Delta E_i \leq 3$ kcal/mol)[e]		100%	100%	100%
P_1[f]		16.3%	39.0%	16.1%
G(+)-conformer	n[d]	122	200	451
	$\sum P_{G(+)}$[e]	6.7%	65.3%	99.8%
G(+), *Z*	n[d]	94	191	
	$\sum P_{G(+)Z}$[e]	6.7%	65.3%	
G(+), *E*	n[d]	28	9	
	$\sum P_{G(+)E}$[e]	0.0%	0.0%	
G(−)-conformer	n[d]	374	294	44
	$\sum P_{G(-)}$[e]	93.3%	34.7%	0.2%
G(−), *Z*	n[d]	281	189	
	$\sum P_{G(-)Z}$[e]	91.3%	5.8%	
G(−), *E*	n[d]	93	105	
	$\sum P_{G(-)E}$[e]	2.0%	28.9%	

[a] Number of conformers screened. [b] Number of conformers of which steric energies were less than 3 kcal/mol from the global minimum energy ($\Delta E_i \leq 3$ kcal/mol). [c] Population of conformers of $\Delta E_i \leq 3$ kcal/mol relative to that of total conformers screened. [d] Number of conformers of which steric energies were less than 50 kcal/mol from the global minimum energy ($\Delta E_i \leq 50$ kcal/mol). [e] Relative population of conformers of $\Delta E_i \leq 50$ kcal/mol. [f] Relative population of conformers at the global minimum energy.

signals of C(16), C(17), C(18), and C(19) of the macrocyclic ring of cytochalasin analogues were not well simulated, we next analyzed the conformations of CCB and CCA in the solution. Their conformations were computed by taking all the possible rotations of the bonds into consideration with use of the MM conformation search program CONFLEX3[12] for cyclic compounds. We screened the conformers with a steric energy ΔE_i at the *i*-th energy level from the ground minimal energy under an energy threshold of 50 kcal/mol, and then optimized their values. Namely, the ΔE_i of the most stable conformer was referred to as ΔE_1 (=0 kcal/mol). As a result, we found that there were 3072 conformers of CCB and 6578 conformers of CCA. Of these conformers, 82 conformers of CCB and 61 conformers of CCA were found to take $\Delta E_i \leq 3$ kcal/mol, and the sums of their populations were very close to 100% (98.8% for CCB and 96.3% for CCA). Therefore, almost all the possible conformers take the steric energy in the energy range up to 3 kcal/mol from the global minimal energy ($\Delta E_i \leq 3$ kcal/mol). In addition, there were 496 conformers of CCB and 494 conformers of CCA at an energy level of less than 50 kcal/mol ($\Delta E_i < 50$ kcal/mol). The results of conformation analyses with the conformers of $\Delta E_i \leq 3$ kcal/mol and those of $\Delta E_i \leq 50$ kcal/mol are summarized in Table 3.

Next, we calculated the population of each conformer P_i, which takes ΔE_i, according to the Boltzmann distribution. The P_i values for conformers with the global minimum energy (P_1) in CCB and CCA were determined as 16.3% and 39.0%, respectively, indicating that in solution only about one-sixth of the CCB molecules and about 40% of the CCA molecules take the same conformation as those in the crystals. This is why the simulated NMR spectra were different from the observed spectra. We calculated the weighed averaged *J* values (J_{ave}) of CCB and CCA statistically, taking into consideration the conformations of 496 conformers of CCB and 494 conformers of CCA at $\Delta E_i \leq 50$ kcal/mol (Table 3), and simulated their NMR spectra, as shown in Figures 1C and 3C, respectively. The signals that had not been simulated well with the use of J_{calc}, such as those of the C(15), C(16), C(17), C(18), and C(19) protons, were improved by simulation with the use of J_{ave}.

As Jung's group[8,9] proposed that the C(20)−C(21)═C(22)−C(23)−O(24) sequence is the most important for binding with the glucose transporter, we paid attention to the orientation of the C(21)═C(22) ethylene with respect to the C(23) carboxyl group (α,β-unsaturated lactone moiety), and that of the C(23) carboxyl group with respect to the 14-membered macrocyclic ring. We found that all the conformers took a dihedral angle of C(21)═C(22)−C(23)−O(24) of approximately either 0° or 180°. A conformer with a 0° dihedral angle is referred to as a *Z*-conformer, and that with a 180° dihedral angle as an *E*-conformer. With CCB, 375 of 496 conformers (relative population $\sum P_i = 98.0\%$) were *Z*-conformers, and the other 121 conformers were *E*-conformers ($\sum P_i = 2.0\%$), indicating that all the C(21)═C(22) ethylene of CCB was conjugated with the C(23) carboxyl group, giving a coplanar structure: the α,β-unsaturated lactone moiety takes a planar structure. The dihedral angle was 0° (=*Z*-conformer) in 380 of 494 conformers of CCA ($\sum P_i = 71.1\%$), and 180° (=*E*-conformer) in the other 114 conformers ($\sum P_i = 28.9\%$).

In addition, the dihedral angles of C(23)−O(24)−C(9)−C(4), namely the orientation of the C(21)═C(22)−C(23)−O(24) plane with the 14-membered macrocyclic ring (see Figures 2 and 4, in which the dihedral angle is shown by an arrow), of the most stable conformers of CCB and CCA were determined to be −70.4° and +71.6°, respectively, showing that at the global minimum energy CCB and CCA take the anticlockwise gauche rotamer (G(−)-conformer) and clockwise gauche rotamer (G(+)-conformer), respectively. Therefore, the orientation of the planar C(21)═C(22)−C(23)−O(24) was parallel to the short axis of the 14-membered ring in the most stable conformer of CCB (Figure 2), but parallel to the long axis in that of CCA (Figure 4). Accordingly, the conformations of cytochalasin analogues are characterized by the combinations of G(−)- and G(+)-conformations with *E*- and *Z*-conformations. However, as C(23)═O of the most stable conformer of CCB is reported to be well superimposable on C(1)−OH of glucose,[9] the conformation of the α,β-unsaturated lactone moiety containing C(23)═O is presumably important for hexose transport inhibition activity. Accordingly, we analyzed analogues having G(−)- and G(+)-conformations.

3. Conformational Feasibility Analyses of Cytochalasins B and A. As the most stable structures of CCB and CCA characteristically take the G(−)- and G(+)-conformations, respectively, we next determined the total populations ($\sum P_i$) of the G(−)- and G(+)-forms from the P_i values. The values determined as $\sum P_{G(-)}$ and $\sum P_{G(+)}$ represent the feasibilities of cytochalasin analogues to take the G(−)- and G(+)-forms, respectively. As described above, the conformer of CCA at the global minimal energy (ΔE_1) was in the G(+)-form. The conformers at the second lowest ΔE_2 (=0.83 kcal/mol) and third lowest ΔE_3 (=0.89 kcal/mol) were found to take the G(+)- and G(−)-form, respectively. The P_1, P_2, and P_3 values of these conformers were determined to be 39.0%, 9.6%, and 8.7%, respectively. Therefore, $\sum P_{G(-)}$ was 8.7% and $\sum P_{G(+)}$ was 48.6%. By this procedure, we computed the P_i values of 496 conformers of CCB and 494 conformers of CCA in which $\Delta E_i \leq 50$ kcal/mol. The values of $\sum P_{G(-)}$ and $\sum P_{G(+)}$ of all possible conformations of CCA were determined to be 34.7% and 65.3%, including 39.0% of the global minimal conformer, respectively. In contrast, as described above, the most stable conformer of CCB took the G(−)-form, and its P_1 value was as low as 16.3%.

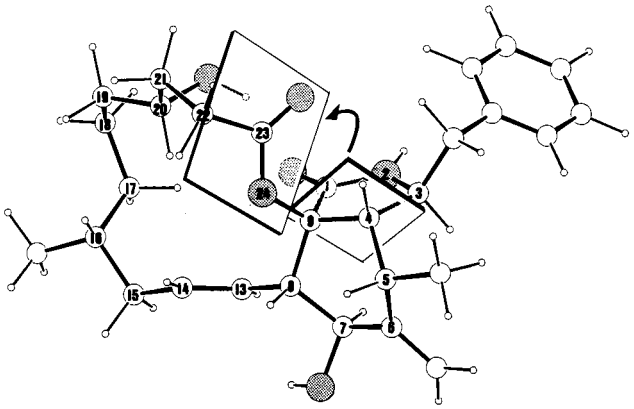

Figure 5. Most stable conformation of $CCBH_2$. Clockwise orientation of the carboxyl moiety with respect to the O(24)−C(9)−C(4) plane is shown by an arrow. For details, see the legend of Figure 2.

The $\sum P_{G(-)}$ and $\sum P_{G(+)}$ values of CCB were determined to be 93.3% and 6.7%, respectively.

4. Conformation of 21,22-Dihydrocytochalasin B. Next, we examined the conformation of the noninhibitory analogue $CCBH_2$, in which the C(21)═C(22) bond of CCB is saturated. As the geometrical data of $CCBH_2$ from X-ray crystallography are not available, we performed MM calculations by the procedure described above. At its global minimum energy, $CCBH_2$ was found to take the G(+)-form. A stereoscopic view of the global minimal conformer of $CCBH_2$ based on the ORTEP model is shown in Figure 5. The dihedral angle of C(23)−O(24)−C(9)−C(4) was +74.0°. The G(−)-conformer was first found at the high ΔE_i of 3.6 kcal/mol, indicating that the stable conformation of $CCBH_2$ was the G(+)-form. Consistent with these results, $\sum P_{G(-)}$ was 0.2%, whereas $\sum P_{G(+)}$ was 99.8% in all the conformers in which $\Delta E_i \leq 50$ kcal/mol. It is noteworthy that C(20)−OH is not conjugated with C(23)═O, and so is not present in the conjugated plane of C(23)−O(24) in either the G(−)- or G(+)-form of $CCBH_2$. The orientation of C(20)−OH in both the G(−)- and G(+)-conformer is quite different from those in the corresponding regions of the G(−)- and G(+)-conformers of CCA and CCB.

Discussion

For deducing the structural features of the cytochalasin analogues CCB and CCA necessary for their hexose transport inhibitions, we performed conformational analyses of CCB and CCA as well as of the ineffective analogue $CCBH_2$ by MM computation. We found that the conformations of cytochalasin analogues were essentially characterized by the orientation of the lactone moiety with respect to the hydrogenated isoindole ring. A conformer in which the lactone moiety is oriented parallel to the short axis is referred to as the G(−)-conformation, and the one in which it is oriented parallel to the long axis is referred to as the G(+)-conformation.

In the potent inhibitor CCB, the α,β-unsaturated lactone moiety is conjugated with the C(20)−OH bond forming a coplanar structure. By conformational analysis computation, the values of $\sum P_{G(-)}$ and $\sum P_{G(+)}$ were determined to be 93.3% and 6.7%, respectively, indicating very high feasibility of CCB to take the G(−)-conformation. This could be because tetrahedral sp^3 C(20), due to its steric effect, easily causes the orientation of the α,β-unsaturated lactone moiety conjugated with the C(23)−OH bond, leading to the parallel conformation to the short axis of the 14-membered macrocyclic ring. In the less inhibitory analogue CCA, conjugation of the α,β-unsaturated lactone moiety with the plane of the C(20) carbonyl group forms a coplanar structure. In this case, the steric hindrance of the C(20) carbonyl group is not great, so the lactone moiety is expected to take the more energetically stable orientation parallel to the long axis of the 14-membered macrocyclic ring. In fact, the value of $\sum P_{G(+)}$ (65.3%) was greater than that of $\sum P_{G(-)}$ (34.7%). In the noninhibitory analogue $CCBH_2$, the α,β-saturated lactone moiety is not conjugated with C(20)−OH, and so the steric effect of C(20)−OH is very small. As a result, the orientation of the lactone moiety is changeable. However, it tends to take the horizontal orientation (G(+)-conformation) to minimize the steric effect of the 14-membered macrocyclic ring, as reflected by the values of $\sum P_{(G(-)}$ and $\sum P_{G(+)}$ of 0.2% and 99.8%, respectively.

From the study of crystal structures, Griffin et al.[9] proposed that the 14-membered macrocyclic ring of CCB binds to the hydrophobic region of the glucose transporter, and the hydrogenated isoindole moiety and C(23)═O of CCB interact with the polar interface region of the transporter. In crystals of CCB and CCA, the heteroatoms N(2) and C(7)−OH were well superimposed on C(6)−OH and C(3)−OH, respectively, of D-glucose. Although C(23)═O of CCB was well superimposed on C(1)−OH of D-glucose, no superimposition of C(23)═O of CCA on C(1)−OH of glucose was observed, and this geometry of C(23)═O was interpreted to result in the lower inhibitory activity of CCA.[9]

From the present study, it is reasonable to conclude that the G(−)-conformation of cytochalasin analogues, in which the orientation of the lactone moiety with respect to the hydrogenated isoindole ring is the same as that of CCB in the crystal structure, is responsible for their hexose transport inhibition. The values of $\sum P_{G(-)}$ of 93.3%, 34.7%, and 0.2% for CCB, CCA, and $CCBH_2$, respectively, correlate well with their inhibitory activities on glucose transport across human erythrocyte membranes (the concentrations of CCB, CCA, and $CCBH_2$ necessary for inhibition are 0.3−0.8, 1.0−4.0, and more than 100 μM, respectively[8]). Therefore, the abilities of cytochalasin analogues to take the G(−)-conformation can be concluded to be directly associated with their transport inhibition activities. The present method was effective for determination of the conformations of cytochalasin analogues necessary for hexose transport inhibition.

Experimental Section

Materials. Cytochalasins B and A were purchased from Sigma Chemical Co. (St. Louis, MO).

NMR Spectroscopy. The 400 MHz ^{1}H NMR spectra of CCA and CCB at 20 mg/mL were obtained on a JEOL GSX-400 spectrometer in pyridine-d_5 with sodium 3-(trimethylsilyl)-1-propanesulfonate-d_4 as an internal standard at room temperature. 2D COSY spectra were recorded with ambient spectral widths with an F2 size of 2 K and an F1 size of 512 W when FIDs were collected, and only the F1 direction was zerofilled to 1 K when they were transformed. Phase-sensitive NOESY spectra were taken with use of a program (NOESYPH) with a pulse delay of 2.4 s. The data size was usually 4 K (F2) × 256 W (F1) when FIDs were collected, and the F1 direction was zerofilled to 1 K when the FIDs were transformed.

Processing of Molecular Geometry. Conformational analysis was performed with the program CONFLEX3, a gift from Prof. E. Osawa, Toyohashi Technology and Science College, according to the procedure reported by his group for systematic searches of stable conformers of cyclic compounds.[12] Structural optimization was performed with the MM2(91) program by Prof. N. L. Allinger[18] distributed by QCPE,

(18) Burkert, U.; Allinger, N. L. *Molecular Mechanics*; American Chemical Society: Washington, DC, 1982.

Indiana University, on a Fujitsu S-4/10 SPARC Workstation, Information Processing Center, University of Tokushima.

X-ray crystallographic coordinates of cytochalasins were taken from the Cambridge Structure Databank of the Computer Center, Tokyo University.[9,14] Projected views of the crystals and computational structures were drawn by the JCPE registered program ORTEPC (P039), revision of C. K. Johnson's ORTEP-II (ORNL-5138) for microprocessor NEC PC9801 by J. Toyoda, Institute of Molecular Sciences, Okazaki.

Calculation of Coupling Constants. A vicinal coupling constant $^3J_{HH}$ with molecular geometry was predicted with a program created by us according to a modified Karplus-type parabolic equation, including not only the traditional steric effect but also terms of the electronic factors, reported by Haasnoot and his colleagues.[15]

$$^3J_{HH(calc)} = K_1 \cos^2 \phi + K_2 \cos \phi + K_3 + \sum \Delta\chi_i \{K_4 + K_5 \cos^2(\xi_i \phi + K_6 |\Delta\chi_i|)\}$$

where K_1-K_6 represent empirical coefficients. The torsion angle ϕ was defined by a Newmann projection of the vicinal protons in each H−C−C−H assembly. The term ξ_i stands for +1 or −1 according to the orientation of the substituent, and $\Delta\chi_i$ stands for the difference in electronegativity between the substituent attached to the H−C−C−H fragment and hydrogen.

The coupling constant $^4J_{HH}$ of the vinyl−allylic proton was estimated by the method of Garbisch,[16] using his Karplus-type parabolic equation, in which the contribution of the π-bond orbital is taken into consideration.

Reported values for the coupling constant $^2J_{HH}$ of geminal protons[17] were used, except those for the experimental coupling constants of the geminal proton of the C(10) atom and the vicinal protons attached to the C(11) and C(24) methyl groups.

The values of J_{ave} were determined by the following equation:

$$J_{ave} = \sum_{i=1}^{n} P_i J_{calc(i)}$$

where P_i is the population of the ith conformer.

Simulation of NMR Spectra. NMR spectra were simulated by a linear combination of Lorentz functions:[17]

$$f(x) = \sum_{i=1}^{n} \sum_{j=1}^{m} \{AW^2\}/\{W^2 + 4(\nu_{ij} - x)^2\}$$

where A is the peak height, W the half-width of the peak, ν_{ij} the frequency of the j-th splitted peak of the i-th proton calculated from values of J_{calc} and the chemical shift δ, and x the spectrometer frequency.

Acknowledgment. The authors are grateful to Prof. Takenori Kusumi and Miss Kiyoko Uno (Institute for Medicinal Resources, Faculty of Pharmaceutical Sciences, University of Tokushima) for valuable discussions on the analyses of ^{1}H-NMR spectra and to Dr. Takiko Daikoku (Faculty of Pharmaceutical Sciences, University of Tokushima) and Mr. Masahiro Niimi, Mr. Hirofumi Nakajima, and Mr. Mikio Takenaka (Fujitsu Co. Ltd.) for construction of a program for simulation of NMR spectra.

JA9632872